Improving Adhesive Bondline Time of Flight Predictions During Autoclave Cure Utilizing Machine Learning

Tyler B. Hudson[1]*, William J. Pankiewicz[2], Finnian P. Day[2]
[1]NASA Langley Research Center, Hampton, VA 23681, USA
[2]NASA Internships and Fellowships
NASA Langley Research Center, Hampton, VA 23681, USA
*Corresponding author, tyler.b.hudson@nasa.gov, (757) 864-3342

ABSTRACT

Composite materials are increasingly being used in aerospace applications due to their superior strength-to-weight ratio compared to commonly used metals. A current limitation to widespread adoption is the certification of adhesively bonded joints. One approach to improving adhesive bonding in composites is accurately measuring the thickness of adhesive bondlines in composite laminates. Precise bondline thickness control is essential for aerospace applications where adhesive layer thickness directly affects joint fracture properties and structural performance. This study focused on implementing machine learning techniques to determine the ultrasonic time of flight (directly correlated to thickness) in adhesive bondlines throughout autoclave cure cycles. A high-temperature (use up to 180°C) ultrasonic scanning system was deployed in an autoclave to provide time of flight data through composite panels. Three experiments were conducted on the curing of 305 mm × 305 mm unidirectional composite panels. In the first experiment, a piecewise function was fit for the temperature correction factor to account for changing autoclave temperatures. Due to deficiencies in the first calibration experiment, a second experiment was run, and the results were used to train a machine learning model. The revised experiment, in combination with the machine learning model, significantly increased the accuracy of the bondline time of flight predictions (~14% error reduced to <1%). Data was processed using the Regression Learner Application in MATLAB®, with a Support Vector Machine selected for the model. The result was a machine learning algorithm capable of reliably quantifying ultrasonic time of flight through adhesive bondlines. The third experiment provided independent test data for the machine learning model, demonstrating that the model produces accurate predictions from data beyond its training set.

1 INTRODUCTION

1.1 Background and Motivation

The use of composite materials within the aerospace industry has increased rapidly due to their superior mechanical performance and reduced weight compared to commonly used metals. Carbon fiber reinforced polymer (CFRP), in particular, has shown significant potential for use in large aircraft structures [1]. The reduced weight of CFRP, along with its corrosion resistance and, to some extent, fatigue resistance, makes it an increasingly desirable material for aircraft applications [2].

A significant challenge for CFRP parts within the industry is the certification of adhesively bonded joints. Unlike metallic aircraft structures, traditional fastening techniques such as riveted or bolted

joints are not as well suited for joining composite parts. Such techniques require drilling holes into the composite, potentially decreasing strength and inducing delamination or other defects [3]. Consequently, adhesive bonding represents an opportunity for CFRP parts to further reduce weight and decrease manufacturing time if certification can be achieved.

The NASA Transformational Tools and Technologies (TTT) project aims to develop computational and experimental tools and technologies to advance the prediction of future aircraft performance. One key objective is developing real-time in-situ cure monitoring technology to improve inspection capabilities for composite parts and provide insight into cure behavior. The objective of this study was to observe adhesively bonded joints between CFRP panels using the in-situ scanning system developed by Hudson et al. [4-7]. In this work, the real-time data produced by the system was used to investigate the adhesive joint during autoclave cure, establishing a method to measure adhesive bondline time of flight (TOF) (directly proportional with thickness).

1.2 Machine Learning in Composites

Machine learning (ML) is a valuable tool being applied to various engineering fields, including engineering risk assessment [8] and material degradation prediction [9]. Many models have been developed to predict tensile material properties such as ultimate yield strength, elongation, and Young's modulus [10].

The increased use of ML and the accumulated knowledge on the subject has made implementing these techniques in composites research feasible. Chen et al. [11] demonstrated how ML models can be trained to distinguish "good" or "bad" composite designs based on Mode I fracture. Wang et al. [12] demonstrated using machine learning to predict mold filling patterns within resin transfer molding (RTM) processes for various composite parts.

To predict the mechanical properties of unidirectional composites, Pathan et al. [13] developed a supervised ML model capable of calculating elastic properties of composites loaded in the transverse plane. The model, compared to Finite Element (FE) simulations from Abaqus Standard, accurately predicted the transverse Young's moduli and transverse shear modulus, along with the transverse normal yield strength of the composite.

1.3 Strength of Adhesive Bonded Joints

The certification of adhesively bonded composite parts is heavily based on fracture resistance/propagation, a critical design parameter in modern aircraft. Structural fractures resulting in sudden and potentially complete part failure leads to significant safety concerns. Consequently, many studies have focused on the relationship between adhesive joints and fracture modes. Marzi et al. [14] demonstrated that increased adhesive thickness led to increased Mode I and II fracture energy. Sarrado et al. [15] found that the fracture toughness of a specimen increased with thicker adhesive layers, as thicker adhesives can develop larger regions of plastic deformation, increasing bond toughness. Wang et al. [16] demonstrated that increased adhesive layer thickness between CFRP and steel increases the fracture energy of the bond, though this depends on the toughness of the adhesive. Tough adhesives led to larger bonded joint enhancements as adhesive thickness increased, while brittle adhesives showed minor improvements with thickness changes.

These findings from these studies suggest a relationship exists between adhesive layer thickness and the fracture properties of bonded CFRP parts. Therefore, understanding and measuring adhesive thickness within bonded joints will be necessary once quantitative relations between adhesive thickness and fracture properties are determined for each specific material/process combination.

1.4 Adhesive Cure Monitoring

Ultrasonic nondestructive evaluation (NDE) is a method commonly used to evaluate adhesive joints and composite parts for defects post-cure. Evaluated defects often include mechanical properties, delamination, or other bonding defects [17-19]. To the authors' knowledge, however, no group has attempted similar ultrasonic NDE analysis over an area of the joint with moving (i.e., raster scanning) transducer during cure. The CFRP curing process involves state changes (gelation: liquid to rubbery state, and vitrification: rubbery to glassy state) within the adhesive layer accompanied by mechanical property changes. Using ultrasonic NDE testing during curing may provide important insight into adhesive bond properties that have not been studied.

In-situ ultrasonic NDE performed by Hudson et al. has demonstrated success in predicting resin porosity based on acoustic wave attenuation [4,5] and monitoring cure of reflowable interface carbon fiber epoxy prepregs during bonding [6]. Ultrasonic TOF data through bonded CFRP laminates may provide additional information such as adhesive and adherend thickness, and resin state properties (degree of cure, acoustic attenuation). Data collected during cure could also generate metrics for adhesive bonds without post-cure NDE, decreasing manufacturing cycle time and costs.

2 EXPERIMENTATION

2.1 Materials and Equipment

To evaluate and develop ultrasonic in-situ methods for measuring adhesive bondline time of flight, three test specimens, hereinafter referred to as Panels A, B, and C, were constructed. Panels B and C consisted of two half-panels pre-cured in a vacuum press then bonded in an autoclave cure cycle using a thermoset adhesive. Panel A was a single half-panel that was not subsequently bonded to another laminate. All adherends were fabricated from IM7G/8552 unidirectional carbon fiber epoxy prepreg manufactured by Hexcel Corporation®†. Each panel measured 305 mm × 305 mm. After primary cure, the half-panels of panels B and C were bonded using FM209-1U epoxy adhesive manufactured by Solvay® (now Syensqo®). The full composite layup underwent an autoclave cure cycle, during which the sample was continuously scanned using the custom in-situ ultrasonic raster scanner detailed in Hudson et al. [4-6].

† The use of trademarks or names of manufacturers in this report is for accurate reporting and does not constitute an official endorsement, either expressed or implied, of such products or manufacturers by the National Aeronautics and Space Administration.

2.2 Composite Laminate Fabrication

All composite half-panels were fabricated using the same process in a vacuum press. The following cycle was used to cure the half-panels:

1. Begin at ambient pressure (0 kPa) and temperature (~23°C)
2. Apply minimum operational pressure (103 kPa), and ramp to 107°C at 2.8°C/min
3. Hold 60 min
4. Apply 689 kPa, ramp temperature to 177°C at 2.8°C/min
5. Hold 120 min
6. Cool to ambient temperature at 2.8°C/min
7. Release pressure to ambient

After primary cure, for panels B and C, the half-panels were bonded together. Note that panel A was not consolidated into a full laminate structure; therefore, no adhesive was used in fabrication. Relevant details distinguishing the differences between panels A, B, and C are listed in Table 1.

Table 1: Panel construction characteristics.

	Panel A	**Panel B**	**Panel C**
Adherend	IM7/8552 $[0]_{26}$	IM7/8552 Top: $[0/45/90/-45]_{4S}$ (32 plies) Bottom: $[0/45/90/-45]_{S}$ (8 plies)	IM7/8552 Top: $[0]_{26}$ Bottom: $[0]_{26}$
Adhesive	N/A	FM209-1U, 7 plies	FM209-1U, 4 plies
Resin bleed condition	No edge dam	Edge dam	No edge dam

Prior to autoclave cure, each panel was placed on a steel tool plate inside a vacuum bag assembly typical of aerospace composites processing. The assembly included a layer of fluorinated ethylene propylene (FEP) release film (Airtech® A4000V) below the panel, a porous release weave (Airtech® Release Ease® 234TFP), a breather weave (Airtech® Ultraweave® 1332), and a vacuum bag (Airtech® Ipplon DP1000) above the panel. A cutout was created in the top of the vacuum bag to enable direct contact between the ultrasonic transducer and the top surface of the already cured half-panel (Figure 1). A thin layer of glycerol (EchoUltrasonics®) was applied to the top of the half-panel to act as an acoustic couplant. The panels were cured using the autoclave cycle defined below:

1. Begin at ambient pressure (0 kPa gauge) and temperature (~23°C)
2. Apply vacuum to panel using vacuum pump (-100 kPa gauge)
3. Simultaneously pressurize autoclave to 175 kPa gauge at 34 kPa/min and ramp temperature to 121°C at 1.7°C/min
4. Hold 90 min
5. Ramp temperature down to 60°C at -1.7°C/min
6. Release pressure
7. Shut off autoclave; passive cooling to ambient temperature

To measure the temperature of the laminate during cure, several thermocouples were attached at different locations on the top surface of the panel. The thermocouples were attached using flash breaker tape and sealant tape to keep them insulated from the autoclave air temperature. Thermocouple data was critical for bondline TOF calculations.

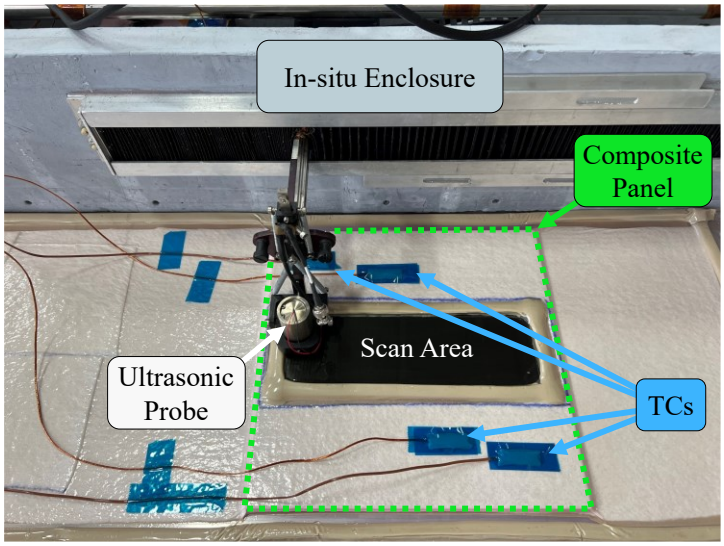

Figure 1: In-situ ultrasonic scanner setup.

2.3 Ultrasonic Inspection

Throughout the cure of the bonded laminates, ultrasonic TOF data was continuously recorded and plotted in real time using the in-situ scanner. The ultrasonic transducer raster scanned a 225 mm × 25 mm area for panels A and C and a 25 mm × 50 mm area for panel B with a 1.0 mm × 1.0 mm resolution per pixel. A full scan was completed approximately every 8 minutes (includes time for saving data at the end of each scan). At each pixel, the 2.25 MHz (center frequency) transducer would measure the ultrasonic wave in pulse-echo mode with 100 averages per pixel. Reflections from various panel interfaces were recorded for each acoustic pulse. Figure 2 depicts these reflections.

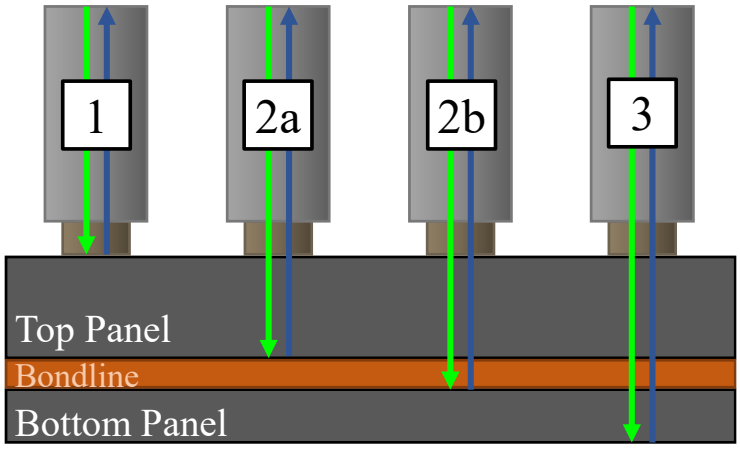

Figure 2: Diagram showing the significant ultrasonic reflections measured by the transducer.

An example A-scan waveform from the in-situ ultrasonic scanner can be viewed in Figure 3. A Hilbert envelope was added to the waveform to help distinguish between the various acoustic reflections. Each reflection corresponds to a different peak along the waveform.

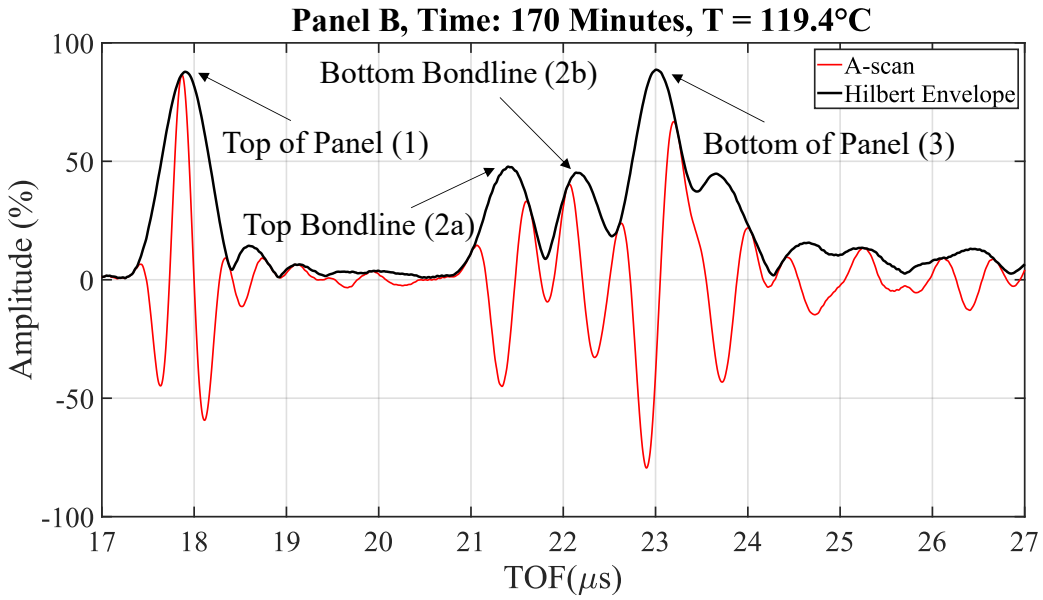

Figure 3: A-scan waveform and envelope from Hilbert transform measured by the in-situ scanner near the center of the scan area (x = 12 mm, y = 112 mm) in panel B.

2.4 Time of Flight Calculation

Using the Hilbert envelope and the ultrasonic pulse reflections, the TOF within the bondline of a laminate can be calculated. The most accurate TOF measurement, hereby denoted as the *Direct Method* (Eq. 1a/b), utilizes the acoustic reflections from the top and bottom of the adhesive bondline. This method is best implemented when the acoustic reflections provide clear amplitude

peaks for the top and bottom of the bondline. For clarity, the nomenclature in Figure 2 and Figure 3 will be used throughout the paper to specify locations within the laminate.

$$TOF_{bondline} = TOF_{bottom\ bondline} - TOF_{top\ bondline} \tag{1a}$$

$$TOF_{bondline} = TOF_{2b} - TOF_{2a} \tag{1b}$$

Of the methods discussed in this paper, the direct method is the most accurate for calculating bondline TOF but becomes more difficult to use as the bondline thickness decreases. With a sufficiently small bondline thickness or high ultrasonic velocity (such as after vitrification), the amplitude peaks from the 2.25 MHz ultrasonic transducer become unclear (Figure 4). The pulses reflected from the top and bottom of the bondline can return to the transducer at close the same time, causing the Hilbert envelopes to merge.

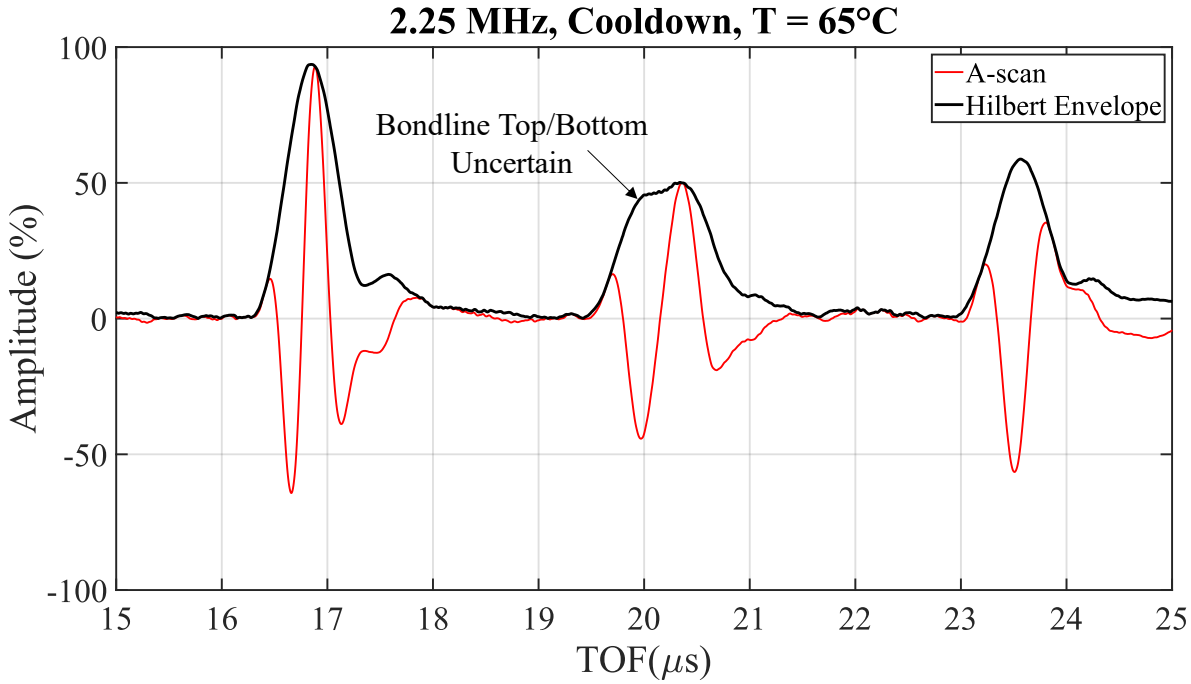

Figure 4: A-scan waveform showing the ambiguity in bondline reflections that can occur at faster sound velocity.

The hardware limitation of the 2.25 MHz transducer required an alternative method for calculating the TOF through the bondline, hereby denoted as the *Subtraction Method* (Eq. 2a/b). The transducer was adequate for resolving the reflection pulse from the top (TOF_1 in Figure 3) and bottom (TOF_3 in in Figure 3) of the laminate (i.e., a pulse that traveled through the entire laminate). This approach calculates the bondline TOF by subtracting the TOF through each isolated half-panel (measured before assembling the bonded laminate) from TOF through the entire laminate at each scan.

$$TOF_{bondline} = TOF_{laminate} - TTCF \times (TOF_{0,top\ panel} + TOF_{0,bottom\ panel}) \tag{2a}$$

$$TOF_{bondline} = (TOF_3 - TOF_1) - TTCF \times (TOF_{0,top\ panel} + TOF_{0,bottom\ panel}) \quad (2b)$$

Precise measurements of the TOF through each half-panel were required to prevent the relatively small bondline TOF (in comparison to the half-panels) from being below the signal to noise ratio of the measurement due to the experimental uncertainty of the larger half-panel TOFs. In a simpler explanation, the subtraction method is an ill-posed problem in that it subtracts two "large" numbers from a larger number to calculate a "small" number. However, the method can work with accurate measurements of the "large" numbers.

To establish precise TOF measurements through each half-panel, each half-panel was ultrasonically inspected at room temperature and atmospheric pressure with no adhesive present and identical boundary conditions as during in-situ data collection (e.g., vacuum bagged to tool plate). These scans created a TOF map over the entire panel area, which could then be subtracted from the real-time through-laminate TOF during cure to evaluate the additional TOF due to the adhesive.

For practical reasons, it was only feasible to scan each half-panel at room temperature and atmospheric pressure prior to the bonding cure cycle. Since the acoustic TOF through the half-panels is influenced by the autoclave environment, a temperature-pressure-dependent function needed to be established to scale the room temperature half-panel TOFs. This function is known as the TOF temperature correction factor (TTCF).

2.5 Temperature Correction Factor Calibration

2.5.1 Initial Calibration Experiment (Panel A)

Initially, to establish an empirical function for the TTCF, a single, already-cured Hexcel® IM7G/8552 half-panel, denoted as panel A, was scanned throughout a representative bonding cycle inside the autoclave using the same in-situ scanning procedure as the bonded laminate. For each scan, the ultrasonic TOF through the entire half-panel was area averaged and normalized against the TOF at room temperature and atmospheric pressure.

This process resulted in a series of points serving as "multipliers" that could determine the half-panel TOF at specific points in the cure cycle by applying them to an initial half-panel TOF. To establish a continuous function, a piecewise function was fit to the collected data to allow the estimation of the adherend TOF at any arbitrary temperature and pressure. The measured data points were fit using a quadratic function for the points within the initial temperature ramp-up, a linear function for the points within the temperature hold, a different quadratic function for the points while cooling down, and a line for the points after pressure release near the end of the cure cycle (Figure 5).

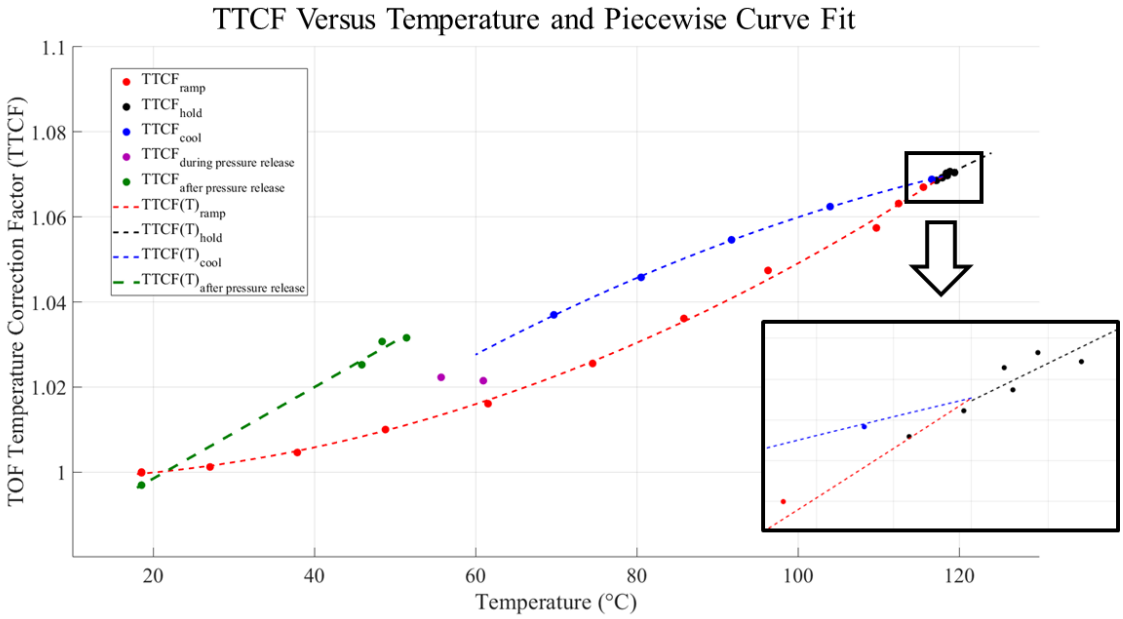

Figure 5: Initial TOF temperature correction factor curve fitting calibration.

The two quadratic functions for temperature ramps (heating and cooling) join at a single point along with the linear function for the temperature hold. To determine which section of the piecewise function to use during data processing, a script was written and implemented using MATLAB® that uses the following decision rules in a series of conditional statements (Eq. 3).

$$TTCF(T,P) = \begin{cases} TTCF_{ramp}(T) = (5.32\times10^{-6})T^2 - (2.39\times10^{-5})T + 0.998 & (T<118,\ \frac{dT}{dt}>0) \\ TTCF_{hold}(T) = (9.27\times10^{-4})T + 0.960 & (T>118) \\ TTCF_{cooldown}(T) = -(4.71\times10^{-6})T^2 + (1.56\times10^{-3})T + 0.951 & (T<118,\ \frac{dT}{dt}<0,\ P>160) \\ TTCF_{pressure\ venting}(T,P) = \frac{P}{689}\times TTCF_{cooldown}(T) + \left(1-\frac{P}{689}\right)\times TTCF_{pressure\ released}(T) & (T<118,\ \frac{dT}{dt}<0,\ 60<P<160) \\ TTCF_{pressure\ released}(T) = (1.08\times10^{-3})T + 0.977 & (T<118,\ \frac{dT}{dt}<0,\ P<60) \end{cases} \quad (3)$$

An additional function piece "$TTCF_{pressure\ venting}$" was defined to accommodate the lack of ultrasound data that could be collected during autoclave pressure venting. The venting process occurs relatively quickly compared to the maximum scanning frequency of the system; thus, insufficient data could be collected to establish an accurate TTCF function during this step of the cure cycle. To resolve this, the TTCF during pressure venting was established as a pressure-weighted average of the cooldown and post-venting functions. Although this rule does not reflect any underlying physics of the system, data collected around this point was deemed insufficient for calibration purposes, and this solution enabled a real-time bondline TOF calculation using a continuous function.

2.5.2 Improved Calibration Experiment (Panel B)

As further bondline TOF experiments were conducted using the TTCF function, it was discovered that the initial calibration produced TOF values that did not make physical sense. For example, in cured composite laminates, acting as solids, TOF is directly proportional to temperature. In some cases, using the initial TTCF calibration function, the calculated TOF in the bondline was inversely proportional to temperature as cooling began and before autoclave pressure release, necessitating another, more accurately calibrated TTCF function.

To establish a more accurate TTCF function, a second calibration experiment was designed and completed, referred to in this paper as panel B. Instead of using a single laminate (half-panel), an experiment was performed with bonded laminate with an adhesive bondline thick enough to ensure both the direct and subtraction methods could be calculated for every pixel for every scan through cure. As with the initial calibration experiment, a TTCF function needed to be developed to calculate bondline TOF. Since the adhesive bondline was thick enough, the direct and subtraction methods could be combined and used to calculate the TTCF at every pixel for every scan. This is known as the *Exact Method* for determining the TTCF. The exact method for calculating the TTCF is given in Eq. 4a/b by solving Eq. 2a for the TTCF.

$$TTCF = \frac{TOF_{laminate} - TOF_{bondline}}{(TOF_{0,top\ panel} + TOF_{0,bottom\ panel})} \tag{4a}$$

$$TTCF = \frac{(TOF_3 - TOF_1) - (TOF_{2b} - TOF_{2a})}{(TOF_{0,top\ panel} + TOF_{0,bottom\ panel})} \tag{4b}$$

To compare the two calibration methods, both were tested with experiment results from panel B. The initial calibration method, using a piecewise function, produced a TTCF of 1.07 at the maximum TOF, with a bondline TOF of 0.636 microseconds. The exact method produced a TTCF of 1.04 at the same point with a bondline TOF of 0.744 microseconds. While the difference between TTCF values is minimal (3% difference), the bondline TOF percent error approaches 14%.

2.5.3 Machine Learning Model Development (Panel B Data)

Most adhesive bondlines will not be as thick as in panel B, thus the subtraction method is still useful as a widely applicable model for other experiments. Due to the complex relationship between temperature, pressure, temperature ramp rate, and TTCF, simple curve-fitting was not chosen to fit the data. Made possible by the expansive number of data points collected, a machine learning (ML) model was chosen as the most applicable fit method for calculating TTCF using temperature, pressure, and temperature ramp rate as inputs.

During the cure of panel B, 124 scans were completed with a scan area 25 × 50 pixels resulting in 155,000 data points. To decrease computing time and reduce experimental noise, the data points were averaged across the scan axis (the 50-pixel direction) reducing the number of data points to 3,100. The 3,100 data points were randomly split into 1,550 points for training and validation and 1,550 points for dependent testing. A 50/50 split between training/validation and dependent test data was used instead of the more traditional 80/20 or 70/30 splits for two reasons. First, the large dataset of 155,000 data points (reduced to 3,100 after averaging) provided sufficient data for effective model training/validation even with the smaller training subset. Second, the nature of the

autoclave cure process generates highly correlated data points within short time intervals, meaning that adjacent data points share similar characteristics. This correlation increases the risk of overfitting if too much similar data is included in the training set. The larger dependent test set helps improved the probability that the model can generalize to new conditions rather than simply memorizing patterns from the training data. All evaluated ML models were trained and validated using 5-fold (80/20 split in each fold) cross-validation on the 1,550 data points in the training data set.

Twenty-eight ML models were trained and evaluated using default hyperparameters and optimization techniques. The evaluation, conducted in the MATLAB® Regression Learner app, used the root mean squared error (RMSE) of the models on the dependent test data [data points not in the training data set, but from the same experiment (panel B)] as an initial determination of potential models (Table 2). The 10 models with the lowest RMSE values were determined to overfit data, as observed by the close following of the predictions to the experimental noise in the response plots. Additional methods to reduce overfitting for these regression techniques were not implemented as accurate models without overfitting were already available from the other regression techniques. For example, the response plot of an overfit model, Gaussian Process Regression (GPR): Rational Quadratic GPR, is shown in Figure 6. The chosen model was the Support Vector Machine (SVM) with a fine Gaussian kernel, which had the lowest RMSE without overfitting the data. The SVM model response plot is shown in Figure 7, which shows a continuous, smooth response prediction throughout cure with overfitting to the noise in the data.

Table 2: RMSE on the dependent test data set of trained ML models.

	Model Type	RMSE (Test)		Model Type	RMSE (Test)
1	Gaussian Process Regression *(Exponential GPR)*	0.00124	**15**	Neural Network *(Narrow Neural Network)*	0.00428
2	Gaussian Process Regression *(Rational Quadratic GPR)*	0.00124	**16**	SVM *(Coarse Gaussian SVM)*	0.00461
3	Gaussian Process Regression *(Matern 5/2 GPR)*	0.00162	**17**	Kernel *(Least Squares Regression Kernel)*	0.00545
4	Tree *(Fine Tree)*	0.00169	**18**	Kernel *(SVM Kernal)*	0.00579
5	Gaussian Process Regression *(Squared Exponential GPR)*	0.00173	**19**	Linear Regression *(Interactions Linear)*	0.00595
6	Ensemble *(Bagged Trees)*	0.00188	**20**	Stepwise Linear Regression *(Stepwise Linear)*	0.00596
7	Neural Network *(Wide Neural Network)*	0.00211	**21**	Linear Regression *(Linear)*	0.00620
8	Tree *(Medium Tree)*	0.00219	**22**	SVM *(Linear SVM)*	0.00626
9	Neural Network *(Medium Neural Network)*	0.00230	**23**	Linear Regression *(Robust Linear)*	0.00634
10	Neural Network *(Trilayered Neural Network)*	0.00232	**24**	SVM *(Quadratic SVM)*	0.00760
11	Support Vector Machine (SVM) *(Fine Gaussian SVM)*	0.00233	**25**	Efficient Linear *(Efficient Linear Least Squares)*	0.01591
12	Neural Network *(Bilayered Neural Network)*	0.00233	**26**	Efficient Linear *(Efficient Linear SVM)*	0.01822

13	Tree *(Coarse Tree)*	0.00283	**27**	Ensemble *(Boosted Trees)*	0.04358
14	SVM *(Medium Gaussian SVM)*	0.00317	**28**	SVM *(Cubic SVM)*	0.93369

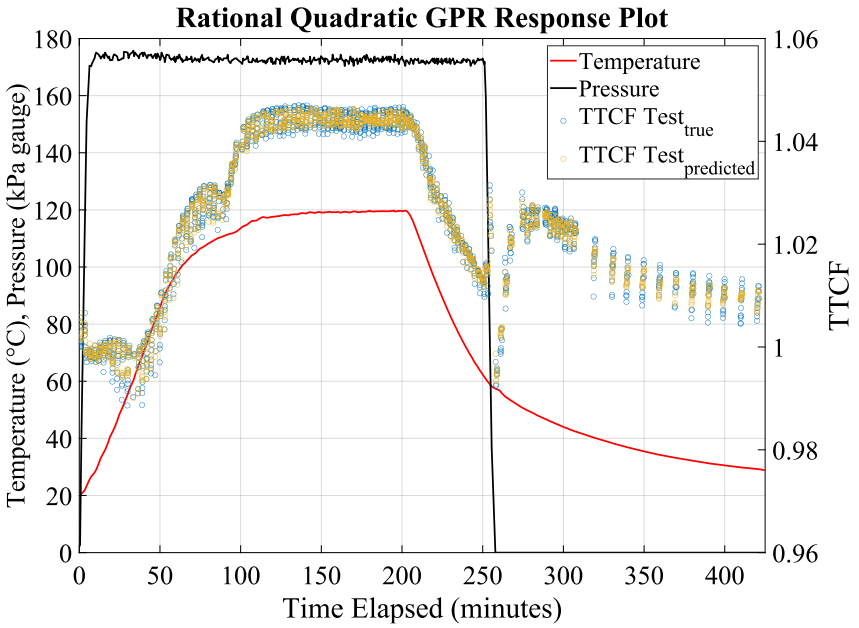

Figure 6: ML model response plot showing overfit data predictions.

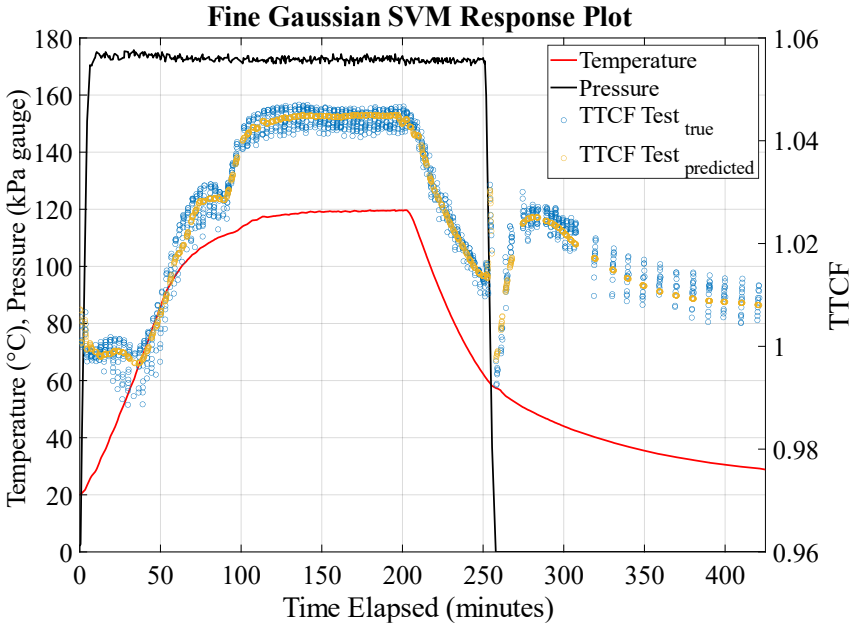

Figure 7: Support Vector Machine (SVM) response plot showing accurate and near-continuous data predictions.

3 RESULTS AND DISCUSSION

3.1 Performance vs. Dependent Test Data

As previously stated, the initial TTCF calibration (derived from panel A data) produced a value near 1.07 at maximum TOF, and the updated calibration (using the improved/more representative experiment from panel B) produced a TTCF value near 1.04. Figure 8 shows the calculated TTCF for panel B throughout the autoclave curing cycle for each of the calibration procedures.

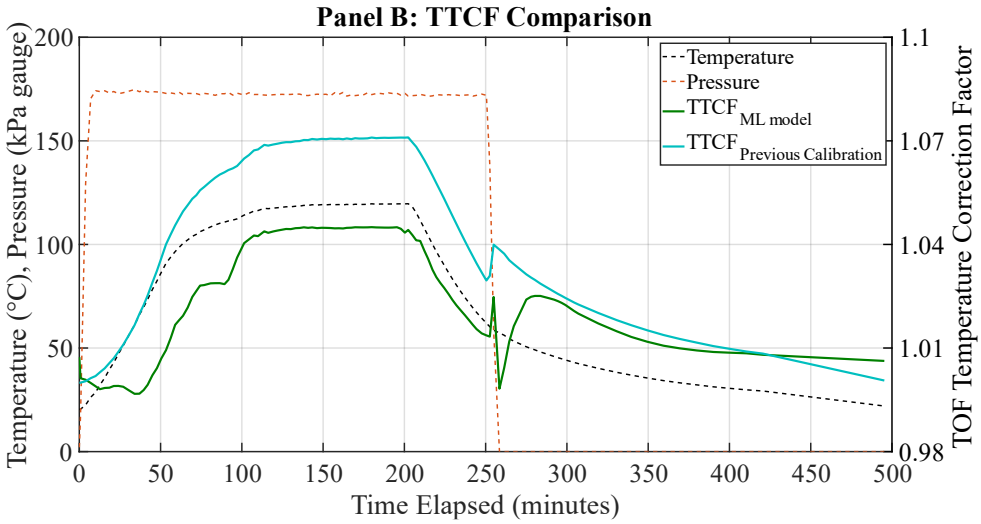

Figure 8: Comparison of the two TTCF calibration methods throughout the cure cycle using panel B test data.

The two TTCF calculation methods can also be compared using the calculated bondline TOF for panel B (Figure 9). compared to the measured bondline TOF using the direct method ($TOF_4 - TOF_3$). The bondline TOF measured using the direct method and the predicted bondline TOF with the ML model are nearly identical, with the only exception occurring at pressure release. In contrast, the initial calibration procedure from panel A significantly deviates from the as measured bondline TOF. This highlights the need for an accurate prediction of the TTCF since relatively small errors in the TTCF prediction are magnified in the bondline TOF prediction.

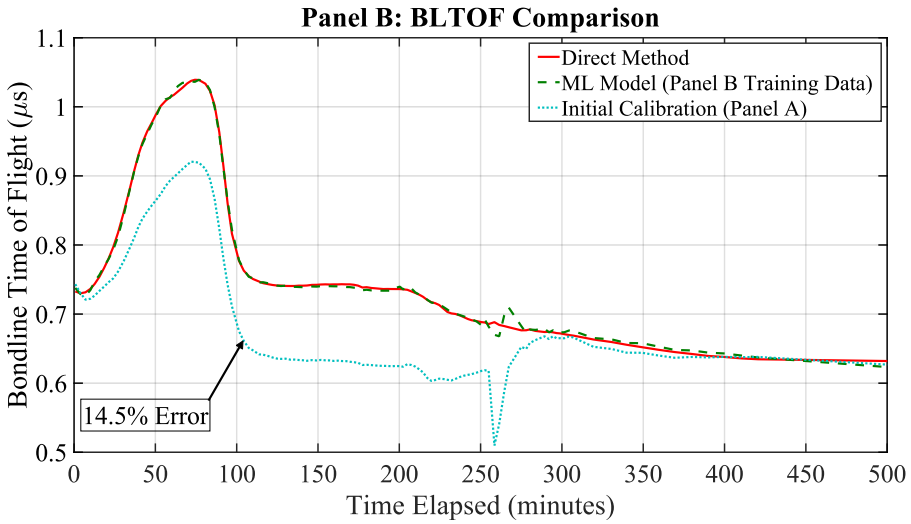

Figure 9: Comparison of bondline TOF (BLTOF) values in panel B throughout the cure cycle.

3.2 Performance vs. Independent Test Data

After training and testing the ML model with dependent test data from panel B, an independent test was run, denoted as panel C, to determine if the ML could accurately predict the TTCF and bondline TOF for an experiment where none of data was in the training data set.

Three individual scans were chosen throughout the autoclave curing process where both direct and subtraction methods could be used to calculate bondline TOF. The chosen scans were taken during temperature ramp roughly 30 minutes into the cure cycle, at maximum TOF, and at the end of the hold directly prior to cooldown.

To determine if the ML model can accurately predict the TTCF for non-training data, and therefore the bondline TOF of independent data, the direct and subtraction methods were plotted against one another (Figure 10). The plotted subtraction method implements the TTCF from the machine learning model.

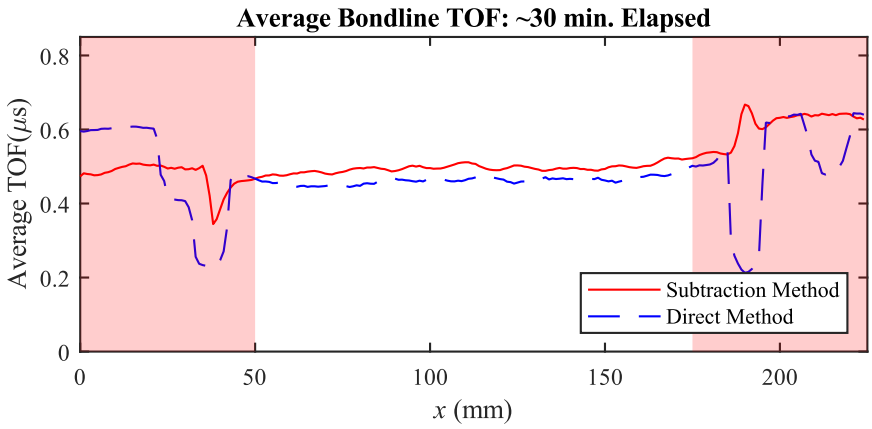

(a)

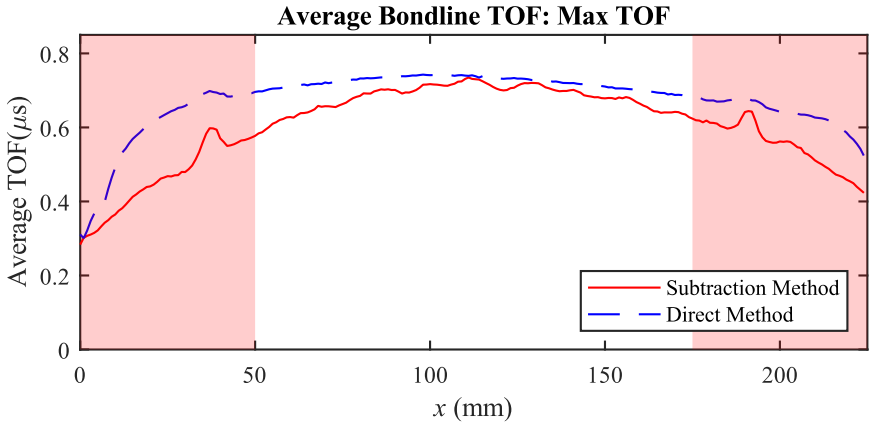

(b)

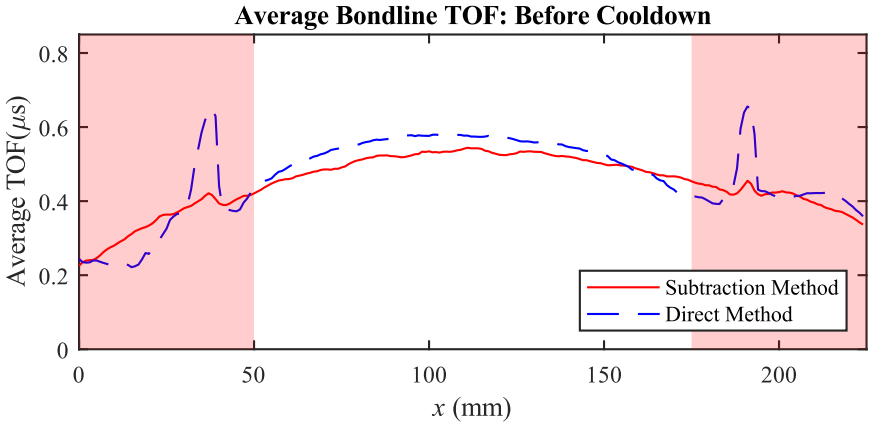

(c)

Figure 10: *y*-averaged bondline thicknesses at significant moments in the cure cycle of panel C; shaded regions correspond to crack starter locations.

The average bondline TOF plots show that the machine learning model can predict adhesive bondline TOF to an acceptable accuracy level. The data from the plots shown above can also be compared quantitatively. Table 3 shows the panel average calculated and predicted TTCF for the scans shown in Figure 10, as well as the percent error between the two values. The calculated

TTCF comes from the exact method while the predicted value is the ML model output. Note that the values taken do not include the crack starter region to present the most accurate data.

Table 3: TTCF average values and percent error at selected scans during the autoclave cure of panel C using ML model.

Cure Cycle Location	Calculated TTCF	Predicted TTCF	Percent Error
~30 min. Elapsed	1.0018	.9970	0.48%
Max TOF	1.0364	1.0437	0.70%
Before Cooldown	1.0396	1.0444	0.46%

The data clearly shows that the ML model accurately predicts the TTCF of the independent test dataset from panel C. The most accurate prediction occurs at the end of the temperature hold, right before cooldown, with the least accurate occurring at maximum TOF, but all are within acceptable limits.

Table 4 lists the scan average bondline TOF for the same scans shown in Figure 10 using the two methods, along with the percent error between them. The direct method is the as-measured value using the reflections from the top and bottom of the bondline (TOF_3 and TOF_4, respectively) while the subtraction method is the predicted value, using the TTCF from the ML model and the reflections from the top and bottom of the laminate (TOF_1 and TOF_2, respectively). As with the TTCF, the values shown do not account for the crack starter region.

Table 4: Bondline TOF average values and percent error at selected scans during the autoclave cure of panel C using ML model.

Cure Cycle Location	Direct Method	Subtraction Method	Percent Error
~30 min. Elapsed	0.463	0.495	6.9%
Max TOF	0.721	0.679	5.8%
Before Cooldown	0.531	0.503	5.3%

As with the TTCF values, the average bondline TOF prediction is most accurate at the end of the temperature hold. The data also demonstrates the necessity of accurately predicting the TTCF when determining adhesive bondline TOF. Small deviations in the correction factor can lead to large errors in TOF calculations.

3.3 Dependent vs. Independent Test Results

The performance of the ML model using both dependent and independent data provides clear direction for model improvement. As expected, the model accurately predicts the TTCF and the bondline TOF throughout the autoclave cure cycle when using dependent data. When presented with independent data, the accuracy of the model is slightly reduced. This could be due to the difference in bondline thickness between the dependent and independent test panels or the layup of the adherends (unidirectional for panel C vs. quasi-isotropic for panel B). One beneficial improvement to the ML model would include adding a panel to the training dataset that has a thinner adhesive bondline, such as the bondline in panel C. This would likely improve the accuracy with thinner bondlines, though it may increase the error in dependent data test results. Before including any data from panel C in the training set, another independent dataset should be generated to test the new model.

4 SUMMARY

The results of this experiment indicated that the improved calibration experiment combined with the chosen machine learning model, the Support Vector Machine with a fine Gaussian kernel, was effective at predicting the TOF temperature correction factor (TTCF) needed to accurately calculate the bondline TOF in a composite laminate during cure. The model proves that using in-situ ultrasonic scanning during autoclave cure is a viable method to compute adhesive bondline thickness in composites once a relationship for ultrasonic velocity can be established. Practically, the model can be implemented in studies focused on determining the timing and extent of adhesive flow during cure and assist studies correlating between bondline thickness and the mechanical properties of carbon fiber composite laminates. As the model was trained on one dataset and tested on another, conducting additional experiments with a wider range of bondline thicknesses, cure cycle profiles, and materials would be beneficial to expand its applicability.

5 BIBLIOGRAPHY

[1] C. Soutis, "Fibre reinforced composites in aircraft construction," *Progress in Aerospace Sciences*, vol. 41, no. 2, pp. 143-151, 2005. https://doi.org/10.1016/j.paerosci.2005.02.004

[2] G. E. Gómez, "Study of carbon fiber reinforced polymers technology and market," *Thesis*, 2022. https://doi.org/10.13140/RG.2.2.27829.45289

[3] M. Aamir, M. Tolouei-Rad, K. Giasin and A. Nosrati, "Recent advances in drilling of carbon fiber-reinforced polymers for aerospace applications: a review," *The International Journal of Advanced Manufacturing Technology*, vol. 105, pp. 2289-2308, 2019. https://doi.org/10.1007/s00170-019-04348-z

[4] T. B. Hudson, P. J. Follis, J. J. Pinakidis, T. Sreekantamurthy and F. L. Palmieri, "Porosity detection and localization during composite cure inside an autoclave using ultrasonic inspection," *Composites Part A: Applied Science and Manufacturing,* vol. 147, 2021. https://doi.org/10.1016/j.compositesa.2021.106337

[5] T. B. Hudson, G. R. Chung, J. J. Pinakidis, P. J. Follis, T. Sreekantamurthy and F. L. Palmieri, "Utilizing an Ultrasonic Inspection System Operating Inside an Autoclave and Machine Learning to Quantify Porosity within Composites During Cure," *Research in Nondestructive Evaluation*, vol. 35(2), 2024. https://doi.org/10.1080/09349847.2023.2277424

[6] T. B. Hudson, F. Baro, A. J. Smith, J. H. Kang, R. J. Cano and F. L. Palmieri, "Ultrasonic Inspection During Autoclave Cure of Reflowable-Interface Composite Joints," *Journal of Composite Materials,* vol. 57(2), 2023. https://doi.org/10.1177/00219983231188173

[7] T. B. Hudson, F. L. Palmieri, A. T. Bryce, J. P. Seebo and E. R. Burke, "Design of an Automated Ultrasonic Scanning System for In-Situ Composite Cure Monitoring and Defect Detection," in SAMPE *2019*, Charlotte, NC, 2019. https://ntrs.nasa.gov/citations/20200002665

[8] J. Hegde and B. Rokseth, "Applications of machine learning methods for engineering risk assessment – A review," *Safety Science*, vol. 122, 2020. https://doi.org/10.1016/j.ssci.2019.09.015

[9] J. Wei, X. Chu, X. Y. Sun, K. Xu, H. X. Deng, J. Chen, Z. Wei and M. Lei, "Machine learning in materials science," *InfoMat*, vol. 1(3), 2019. https://doi.org/10.1002/inf2.12028

[10] A. Stoll and P. Benner, "Machine learning for material characterization with an application for predicting mechanical properties," *GAMM-Mitteilungen*, vol. 44(1), 2021. https://doi.org/10.1002/gamm.202100003

[11] C. T. Chen, G. X. Gu, "Machine learning for composite materials," *MRS Communications*, vol. 9(2), 2019. https://doi.org/10.1557/mrc.2019.32

[12] Y. Wang, S. Xu, K. H. Bwar, B. Eisenbart, G. Lu, A. Belaadi, B. Fox and B. X. Chai, "Application of machine learning for composite moulding process modelling," *Composites Communications*, vol. 48, 2024. https://doi.org/10.1016/j.coco.2024.101960

[13] M. V. Pathan, S. A. Ponnusami, J. Pathan, R. Pitisongsawat, B. Erice, N. Petrinic and V. L. Tagarielli, "Predictions of the mechanical properties of unidirectional fibre composites by supervised machine learning," *Scientific Reports*, vol. 9, 2019. https://doi.org/10.1038/s41598-019-50144-w

[14] S. Marzi, A. Biel and U. Stigh, "On experimental methods to investigate the effect of layer thickness on the fracture behavior of adhesively bonded joints," *International Journal of Adhesion and Adhesives*, vol. 31(8), 2011. https://doi.org/10.1016/j.ijadhadh.2011.08.004

[15] C. Sarrado, A. Turon, J. Costa and J. Renart, "An experimental analysis of the fracture behavior of composite bonded joints in terms of cohesive laws," *Composites Part A: Applied Science and Manufacturing*, vol. 90, 2016. https://doi.org/10.1016/j.compositesa.2016.07.004

[16] Z. Wang, C. Li, L. Sui and G. Xian, "Effects of adhesive property and thickness on the bond performance between carbon fiber reinforced polymer laminate and steel," *Thin-Walled Structures*, vol. 158, 2021. https://doi.org/10.1016/j.tws.2020.107176

[17] B. Yilmaz and E. Jasiuene, "Advanced ultrasonic NDT for weak bond detection in composite-adhesive bonded structures," *International Journal of Adhesion and Adhesives*, vol. 102, 2020. https://doi.org/10.1016/j.ijadhadh.2020.102675

[18] F. Bastianini, A. Di Tommaso and G. Pascale, "Ultrasonic non-destructive assessment of bonding defects in composite structural strengthenings," *Composite Structures*, vol. 53(4), 2001. https://doi.org/10.1016/S0263-8223(01)00058-7

[19] P. Mylavarapu and E. Woldesenbet, "Non-destructive characterization of bondlines in composite adhesive joints," *Journal of Adhesion Science and Technology*, vol. 20, 2006. https://doi.org/10.1163/156856106777412455